Supporting Information

3D-Printed Dual-Polarity Polymer Composites for Broad-Spectrum Volatile Organic Compounds (VOC) Detection

Sri Vaishnavi Thummalapalli[1], Dhanush Patil[1], M. Taylor Sobczak[1], Arunachalam Ramanathan[1], Natalie Crutchfield[2], Libin Yang[1], Varunkumar Thippanna[1], Qixuan Xiang[1], Chao Sui[1], Elizabeth J. Brisbois[2], Hitesh Handa[2,3], Arunchala Nadar Mada Kannan[4], and Kenan Song*[,5]

[1]Mechanical Engineering, College of Engineering, University of Georgia, 302 E. Campus Rd, Athens, Georgia, 30602, USA
[2]School of Chemical, Materials & Biomedical Engineering, College of Engineering, University of Georgia, Athens, Georgia, USA 30602
[3]Department of Pharmaceutical & Biomedical Sciences, College of Pharmacy, University of Georgia, Athens, GA, 30602, USA
[4]The Polytechnic School, Ira Fulton Schools of Engineering, Arizona State University, Mesa, Arizona, USA, 85212
[5]Associate Professor of Mechanical Engineering, School of Environmental, Civil, Agricultural and Mechanical (ECAM) and School of Chemical, Materials, and Biomedical Engineering (CMBE), University of Georgia, Athens, GA, USA 30602, Email: kenan.song@uga.edu

Contents

List of Figures

List of Tables

1 Experimental Section

1.1 Materials

Polyvinyl alcohol(i.e., PVA 3–85 with a molecular weight (Mw) of $\sim$ 54.8 kg/mol, 84.2–86.2%mol degree of hydrolysis, and CAS 9002-89-5) was requested and provided by Kuraray. Cellulose acetate butyrate (CAB) was received from Sigma Aldrich with an average molecular weight of 70,000 g/mol. Multi-walled carbon nanotubes (MWCNTs), NC7000 series, 90% purity, with a surface area of 250–300 m2/g and an average length and diameter of 1.5 μm and $\sim$ 9.5 nm, respectively) were purchased from Nanocyl. Dimethylformamide (DMF) (Anhydrous, 99.5%, CAS 67-68-5) solvent was purchased from Sigma–Aldrich and used as received. All the materials were used as received.

1.2 Feedstock Formulation

To prepare the polymer feedstocks, polyvinyl alcohol (PVA) and cellulose acetate butyrate (CAB) were each dissolved separately in N,N-dimethylformamide (DMF), which served as a common solvent for both polymers. For each polymer, a 10 wt% solution was prepared by dissolving the appropriate amount of PVA or CAB in DMF under continuous stirring. PVA was stirred at 70°C for 8 hours, while CAB was dissolved at 60°C for 3 hours to ensure complete dissolution and homogeneity. After preparing the individual solutions, PVA and CAB were blended together in various volume ratios, specifically 90:10, 80:20, 70:30, and 60:40 (PVA:CAB). Among these, the 60:40 ratio was chosen for subsequent experiments, as this composition exhibited superior miscibility, a slower solidification rate, and a longer shelf life compared to the other blends, which facilitated better handling and processing. The 60:40 blend was further mixed at 40°C for 2 hours to achieve a uniform solution. For the preparation of polymer nanocomposites, MWCNTs were first dispersed in DMF using bath sonication for 12 hours to promote stable and uniform dispersion. The sonicated MWCNT suspension was then added to the 60:40 PVA/CAB blend to achieve final MWCNT loadings of 0.5, 1, 2, and 3 wt% relative to the total polymer content. The resulting composite solution was stirred at 40°C for an additional hour to ensure even distribution of the nanotubes throughout the polymer matrix, further followed by speed mixing at high speeds using a speed mixer set at 2000 rpm for 45 seconds for better dispersion.

1.3 Direct Ink Writing

The feedstock prepared as described in the previous sections was utilized for 3D printing to develop thin films. Direct ink writing (DIW) was employed as the technique for printing the composite inks. The inks were loaded into 10 ml syringes, which were then mounted onto a custom 3D-printed holder. This holder was connected to one of the printhead rails inside the 3D printer (System 30 M, from Hyrel 3D), allowing the setup to follow the imported G-code and achieve autonomous manufacturing.

The choice of an 18-gauge nozzle diameter tip (equivalent to a 1.2 mm needle diameter)

was crucial for ensuring the printability of the various copper-loaded inks. This specific nozzle type provided precise control over ink flow and deposition. To maintain a continuous and uninterrupted ink flow and prevent clogging, a pneumatic fluid dispenser, the Metcal DX-255, was used. This pressure delivery system was essential in preserving deposition precision, preventing metal particle agglomeration, and ensuring the integrity of the resulting films.

Printing pressures and speeds were systematically adjusted, and the inks were printed as films onto glass substrates. The films were allowed to dry in an argon atmosphere for 5 to 8 hours to facilitate solvent evaporation. This meticulous process resulted in the creation of freestanding films characterized by distinct filler combinations. The printing pressure, measured in pounds per square inch (PSI), was a critical factor influencing the ink flow rate and, consequently, the rate of deposition. By employing the DIW approach, we benefited from the flexibility to adjust printing height and execute prints with one or more layers. Fine-tuning printing pressure and speeds was essential for achieving the desired solid loading and optimizing the printability characteristics of the films.

1.4 Characterization

1.4.1 Attenuated Total Reflectance-Fourier Transform Infrared (ATR-FTIR) Spectroscopy

Attenuated Fourier transform infrared spectroscopy (ATR-FTIR) analysis was performed using a Spectrum Two spectrometer from PerkinElmer (Greenville, SC), which collected absorbance readings in the infrared range of 4000 to 500 cm^{-1} at a resolution of 4 cm^{-1} averaged over 64 scans for both pure and blended polymer samples.

1.4.2 Surface Wettability Evaluation

The effects of PVA and CAB blending were evaluated using an Ossila Contact Angle Goniometer (Model: L2004A1). PVA is relatively hydrophilic, whereas CAB is hydrophobic, and blending may induce some changes to surface wettability. Moreover, PVA incorporation is also known to influence the surface wettability of hydrophobic CAB. A droplet of DI water (10 μL) was placed on the composite surface, and the static water contact angle was recorded.

1.4.3 Thermogravimetric Analysis (TGA)

TA Instruments TGA 550 was used to analyze the thermal stability of the formed foams, with thermal degradation temperatures used as reference data for further tests. Each test was conducted from room temperature (RT) to 900°C at a ramp rate of 10 °C min^{-1} with a sample size of 10 mg on a high-temperature platinum (Platinum 635 636 HT) pan.

1.4.4 Differential Scanning Calorimetry (DSC)

The thermal degradation data obtained from TGA was utilized as a reference to define upper temperature for the DSC runs. These analyses were conducted utilizing the TA Instrument Q20 under a nitrogen atmosphere. These tests aimed to determine various phase change temperatures, including the melting temperature (T_m) and crystallization temperature (T_c). In our study, the baseline in DSC experiments was established using an empty pan or an inert reference material, defining the baseline as zero to isolate and quantify the heat flow associated with sample transitions or reactions. The samples were initially equilibrated to a temperature of 30°C and then subjected to a heating cycle from 30°C to 200°C at a rate of 10°C per minute, followed by the same cooling rate to return to the initial temperature of 30°C.

1.4.5 Rheology

The rheological properties of solutions containing PVA/CAB/DMF with varying CNT concentrations were investigated using a 40 mm cone and plate rheometer equipped with a Peltier plate (Discover hybrid rheometer HR 2, TA Instruments). Approximately 2 ml of sample volume was used to maintain uniformity across the tests running each sample three times to minimize error. The viscoelastic characteristics of the PVA/CAB polymer blend solution with different CNT concentrations were examined from room temperature to 80°C. Viscosity measurements were conducted over a shear rate range of 0.1 to 100 s^{-1}, while storage and loss moduli were determined across an angular frequency range of 0.1 to 100 rad s^{-1}. All tests were performed at room temperature.

1.4.6 Scanning Electron Microscopy

The surface morphology of the fabricated composites was studied using field emission scanning electron microscopy (SEM, FEI Teneo, FEI Co.). The samples were coated with 10 nm of gold–palladium using a Leica sputter coater. The imaging was performed at an accelerating voltage of 20.0 kV.

1.4.7 UV-Vis Spectroscopy

Optical properties of the pure and blended polymer films were examined using a Thermo Scientific Genesis 10 S UV–visible spectrophotometer. Initially, baseline correction was performed using the pure solvent (ethanol) in the quartz cuvette for the pure PVA film, ensuring accurate reference subtraction. The pure PVA film was then exposed to ethanol vapor at controlled time intervals to monitor spectral changes induced by gas interactions. Subsequently, the blended polymer film (PVA3/CAB1) was subjected to a similar exposure protocol using three representative solvents ethanol, toluene, and hexane, chosen for their differing polarities. Following each exposure, UV-Vis spectra were collected to evaluate absorbance shifts and assess the influence of gas-polymer interactions on the optical band gap and structural rearrangements within the films.

1.5 Fabrication of PVA/CAB/MWCNT electrodes, and electrical/sensing measurements

The electrode was prepared by attaching conductive copper wires to the PVA/CAB/CNT sample surfaces via silver paste adhesive. The sensitivity of the fabricated devices was measured by a Keithley DMM7510 7 1/2 digital multimeter. All sensing responses were analyzed by measuring the resistance change across the two contacts when exposed to analytes. The chemical sensing measurements were conducted using an in-house designed experimental set-up as shown in **Figure ??(a)**. Volatile organic compound vapors were generated by blowing controlled flows of dry clean air through it at a controlled flow rate of 10, 30, 50, 80, and 100 ml/min into a bubbler filled with 20 ml of selected solvent. The VOC generation rate was calculated by measuring the mass change over certain periods. The solvent mass loss, mass_{loss}, was separately calibrated with controlled Vvoc for 30 min (methanol, ethanol, acetone, benzene, hexane and toluene). The organic solvent containing gas flow was diluted with pure dry clean air, V_{air}, and the total gas flow through the chamber containing the sensor was controlled at 200 $\text{mL}\,\text{min}^{-1}$. Different concentrations were obtained by varying the ratios between V_{air} and V_{VOCs}. The concentration of vapors in ppm (weight to volume concentration of the VOCs) was calibrated by calculating the weight loss of the VOCs at different bubbling rates for 30 minutes at room temperature (RT). For sensing measurements at different temperatures, the methanol bath was heated by placing the bubbler on a hot plate and bubbled at a constant flow rate (150 ppm).

2 Solubility Parameter (δ) of the Blend

2.1 Flory–Huggins Interaction Parameter (χ_{12}) with Solvents

The Flory–Huggins interaction parameter between a solvent and a polymer blend is calculated using:

$$\chi_{12} = \frac{V_m}{RT}(\delta_{\text{solvent}} - \delta_{\text{blend}})^2 \tag{1}$$

where:

- V_m = molar volume of the solvent (in cm^3/mol)
- R = universal gas constant = $8.314\,\text{J/mol}\cdot\text{K}$
- T = temperature (typically $298\,\text{K}$)
- δ_{solvent} and δ_{blend} are in $\text{MPa}^{0.5}$

Solubility Parameter (δ) of the Blend

The solubility parameter of a polymer blend is calculated as a volume-weighted average of its components:

To compare these with the single-parameter solubility parameter δ , the following relationship is used:

$$\delta_{\text{total}} = \sqrt{\delta_d^2 + \delta_p^2 + \delta_h^2} \tag{2}$$

For PVA, the Hansen Solubility Parameter (HSP) values are typically around [1]:

$$\sqrt{(17.0)^2 + (9.0)^2 + (18.0)^2} = \sqrt{289 + 81 + 324} = \sqrt{694} \approx 26.4\ \text{MPa}^{0.5}$$

$$\delta_{\text{PVA}} = 26.4\,\text{MPa}^{0.5}$$
$$\delta_{\text{CAB}} = 22.2\,\text{MPa}^{0.5}$$

For the PVA3/CAB1 (3:1) blend:

$$\delta_{\text{PVA3/CAB1}} = \frac{3 \cdot 26.4 + 1 \cdot 22.2}{3} \approx 25.3\,\text{MPa}^{0.5}$$

Flory–Huggins interaction parameter (χ_{12}) further refines miscibility prediction by incorporating enthalpic interactions between solvent and polymer. A lower χ_{12} (ideally smaller

than 0.5) suggests favorable mixing[2], while higher values indicate poor compatibility and potential phase separation. In the context of PVA/CAB blend processing, using solvents with low χ_{12} (like DMF or ethanol) promotes better dissolution of both polymers[3], resulting in improved film morphology, whereas water (3.678) and toluene (2.173) show strong thermodynamic incompatibility[4,5].

Table S1: Physicochemical properties of selected solvents and their compatibility with the PVA/CAB polymer blend. Solubility parameters (δ), Flory–Huggins interaction parameters (χ_{12}), vapor pressures, and boiling points are listed to assess solvent–polymer miscibility.

Solvent	**Solubility Parameter** δ, **(MPa$^{0.5}$)**	**Flory-Huggins** χ_{12}	**Vapor Pressure (kPa, 20 °C)**	**Boiling Point (°C)**	**Miscibility**
DMF	24.8[6]	0.0078	0.36[7]	153.0[7]	Excellent
Water	47.8[8]	3.678	2.34[9]	100.0[9]	Poor
Ethanol	26.6[10]	0.039	5.80[11]	78.4[10]	Good
Acetone	19.9[12]	0.8592	24.6[13]	56.2[14]	Moderate
Toluene	18.2[5]	2.173	2.90[15]	110.6[15]	Poor

2.2 Water Contact Angle on CAB, PVA and CAB/PVA Surfaces

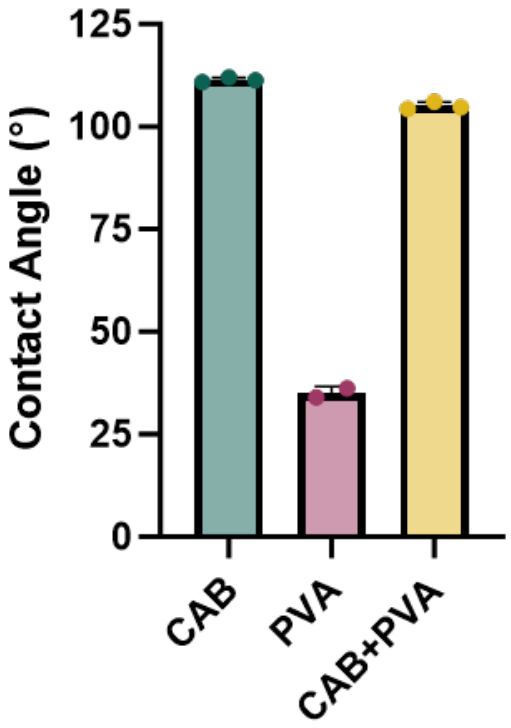

Figure S1: Static water contact angle images for pure CAB ($110 \pm 2°$), pure PVA ($32 \pm 3°$), and representative PVA/CAB blends: PVA1/CAB1 ($95 \pm 4°$), PVA2/CAB1 ($98 \pm 3°$), PVA3/CAB1 ($103 \pm 2°$), and PVA4/CAB1 ($88 \pm 3°$). Colored dots represent individual measurements ($n = 3$).

2.3 Flexibility and Morphology of PVA and PVA/CAB Samples

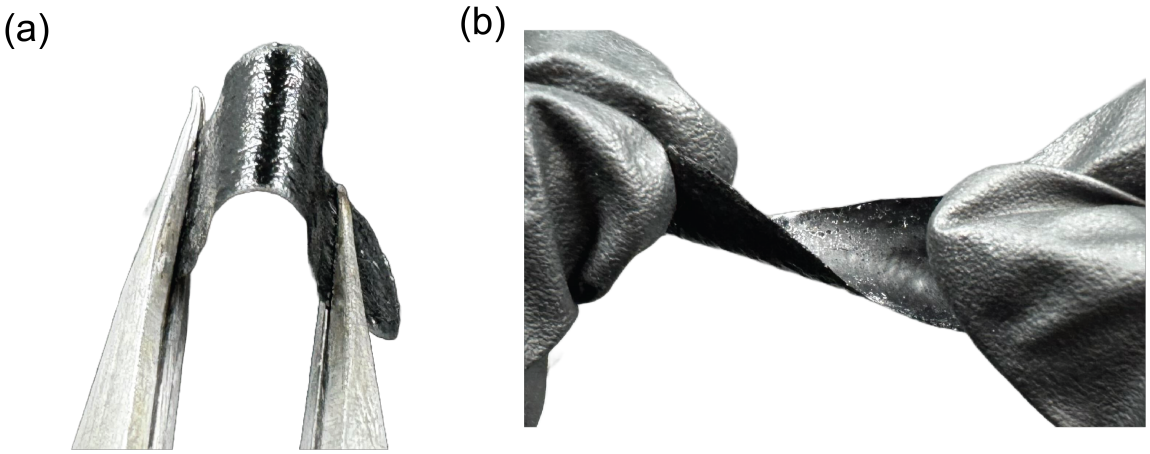

Figure S2: Photographs of the PVA3/CAB1/MWCNT03 composite film fabricated by Direct Ink Writing (DIW) under (a) bending and (b) twisting configurations, demonstrating mechanical flexibility without fracture or delamination.

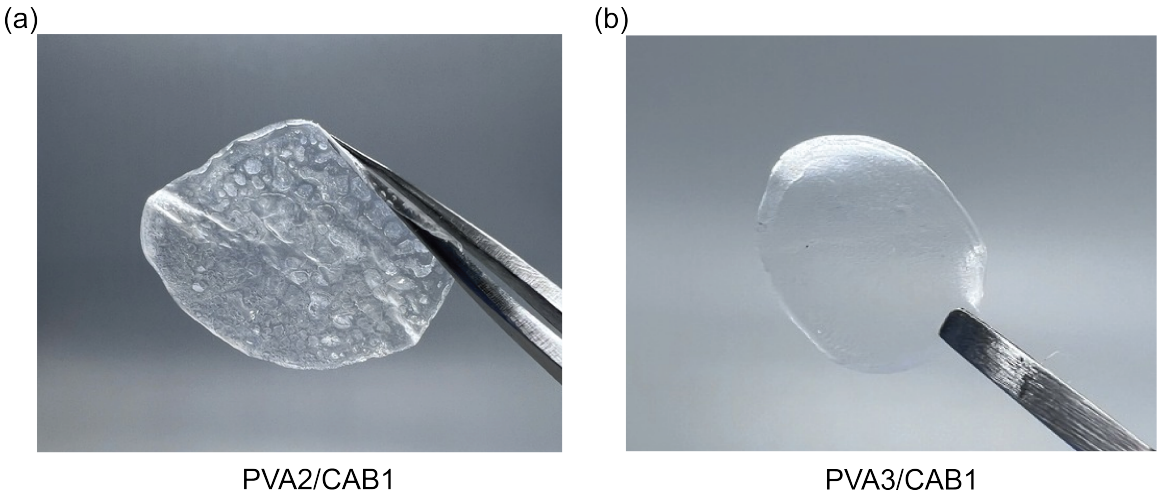

Figure S3: Optical images of (a) PVA2/CAB1 and (b) PVA3/CAB1 blend films showing differences in surface homogeneity and transparency.

2.4 Optical Properties of PVA and PVA/CAB Samples

Table S2: Estimated optical band gap (E_g) and corresponding spectral shifts observed in pure and blended PVA/CAB films. The results highlight how blend composition and solvent vapor exposure influence electronic transitions, with trends indicating red- or blue-shifts in optical absorption depending on polymer dominance and solvent polarity.

Sample	**Estimated E_g (eV)**	**Result / Spectral Behavior**
PVA	∼5.32	Sharp absorption onset, furthest blue-shifted
PVA3/CAB1	∼5.20	Dominated by PVA, blue-shift retained
PVA2/CAB1	∼5.14	Slight red-shift from PVA-rich base
PVA1/CAB1	∼5.09	Higher CAB content → lower E_g
PVA (EtOH)	∼4.98	Minor red-shift from EtOH exposure
PVA3/CAB1_60min (EtOH)	∼4.70	Greater exposure reduces band gap significantly
PVA3/CAB1_60min (Toluene)	∼5.13	Moderate retention of band gap; minor shift
PVA3/CAB1_60min (Hexane)	∼4.97	Minimal effect from non-polar hexane

2.5 Sensitivity of PVA and PVA/CAB blend samples as compared with literature reports

Table S3: Comparative summary of chemiresistive gas sensors based on single and blended polymer matrices combined with various fillers, evaluated for both polar and non-polar gases at a fixed concentration of 100 ppm.

S.No	Polymer Matrix	Filler Type	Gas Type	Sensitivity (%)	Response Time (s)	Recovery Time (s)	Reference
1	PVA	PPY	Ethanol	72	42	200	[16]
2	PANI	In_2O_3	NH_3	46	118	144	[17]
3	PANI/P3HB	SnO_2	Ethanol	200	300	600	[18]
4	PLA/SAN	MWCNT	Ethanol	17	200	800	[19]
5	PVA/PANI	CNF	NH_3	83	46	62	[20]
6	PANI/Cellulose	TiO_2	NH_3	9	200	900	[21]
7	PLA/SAN	MWCNT	Toluene	6.5	200	1100	[19]
8	PVA/CAB	MWCNT	Ethanol	9.5	95	150	This work
9	PVA/CAB	MWCNT	NH_3	11	80	100	This work
10	PVA/CAB	MWCNT	Toluene	3	180	200	This work

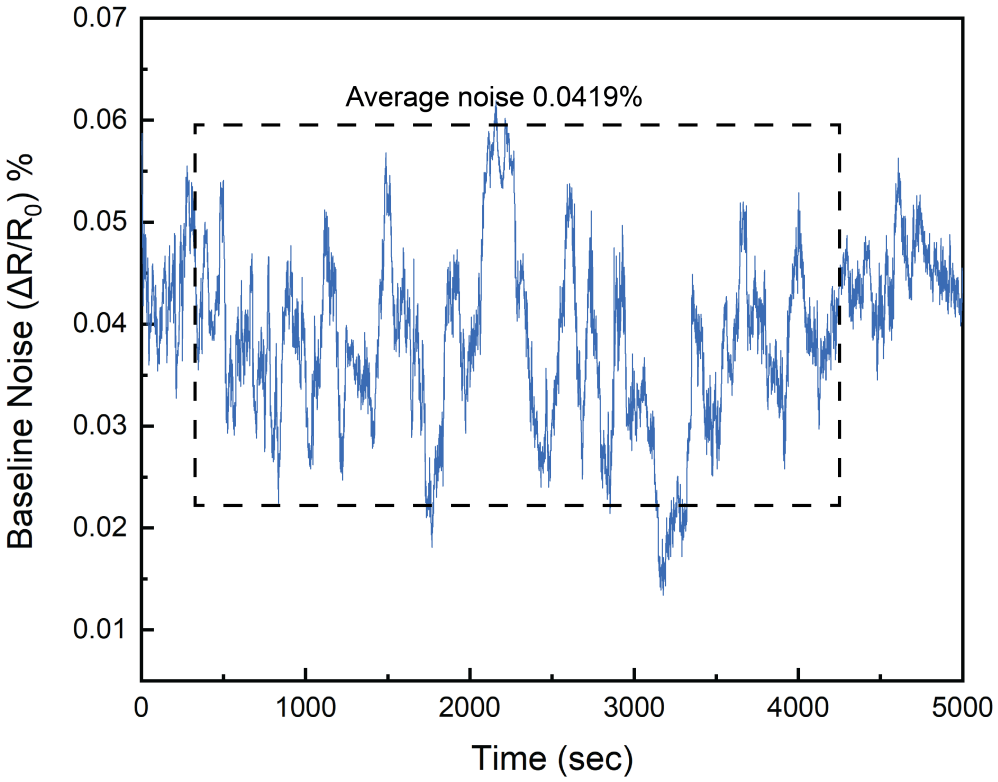

Figure S4: Baseline resistance noise ($\Delta R/R_0$) of the PVA3/CAB1/MWCNT03 sensor recorded over 5000 s in clean air at room temperature, with an average noise level of 0.042%.

Figure S5: Photographs of a pure PVA/MWCNT composite film after exposure to elevated conditions (∼50 °C and 70% RH), showing visible warping and shrinkage.

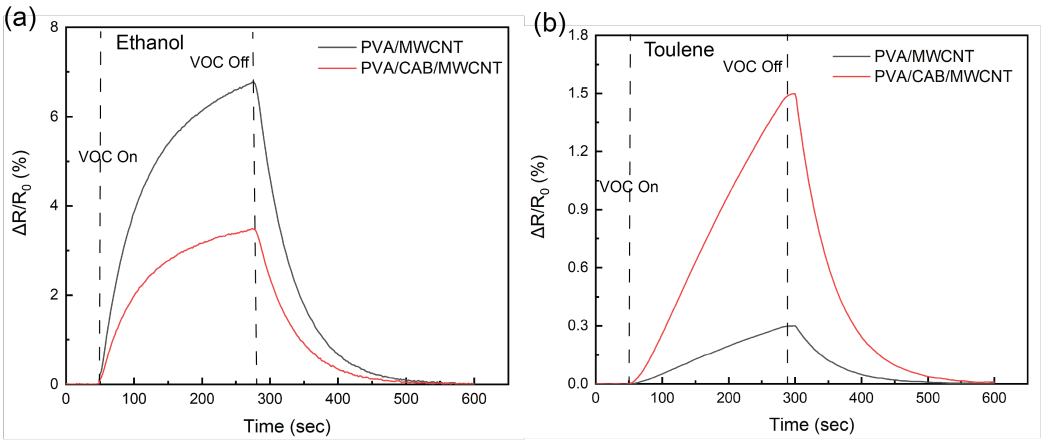

Figure S6: Component-controlled sensing comparison between PVA/MWCNT (no CAB, black) and PVA3/CAB1/MWCNT03 (red) under Protocol A (VOC ON: 50–280 s), $n = 3$ replicates per composition. (a) Time-resolved $\Delta R/R_0$ for ethanol (50 ppm): PVA/MWCNT 6.8% vs PVA3/CAB1/MWCNT03 3.5%. (b) Time-resolved $\Delta R/R_0$ for toluene (100 ppm): PVA3/CAB1/MWCNT03 1.5% vs PVA/MWCNT 0.3%.

PVA/MWCNT shows the larger response (6.8% vs 3.5%), confirming that PVA hydroxyl groups dominate the polar VOC sensing pathways.PVA3/CAB1/MWCNT03 shows the larger response (1.5% vs 0.3%), confirming that CAB ester domains enable non-polar VOC sensing. The crossover between panels (a) and (b) is the direct mechanistic signature of dual-polarity sensing within a single experimental dataset.

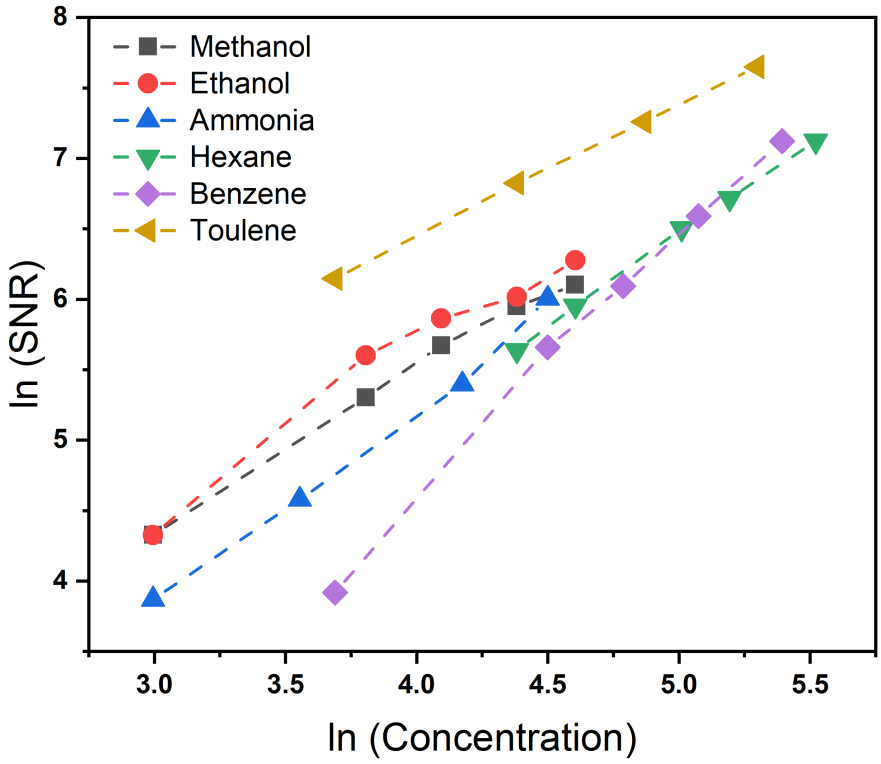

Figure S7: Log-log (ln–ln) plot of signal-to-noise ratio (SNR) versus analyte concentration for the PVA3/CAB1/MWCNT03 sensor. Power-law fits (SNR $= a \cdot C^n$): Toluene ($a =$ 15.11, $n = 0.93$, $R^2 = 0.9995$); Methanol (2.68, 1.13, 0.993); Ethanol (2.34, 1.20, 0.967); Hexane (0.94, 1.30, 0.999); Ammonia (0.71, 1.40, 0.994); Benzene (0.054, 1.88, 0.995). All $R^2 \geq 0.97$.

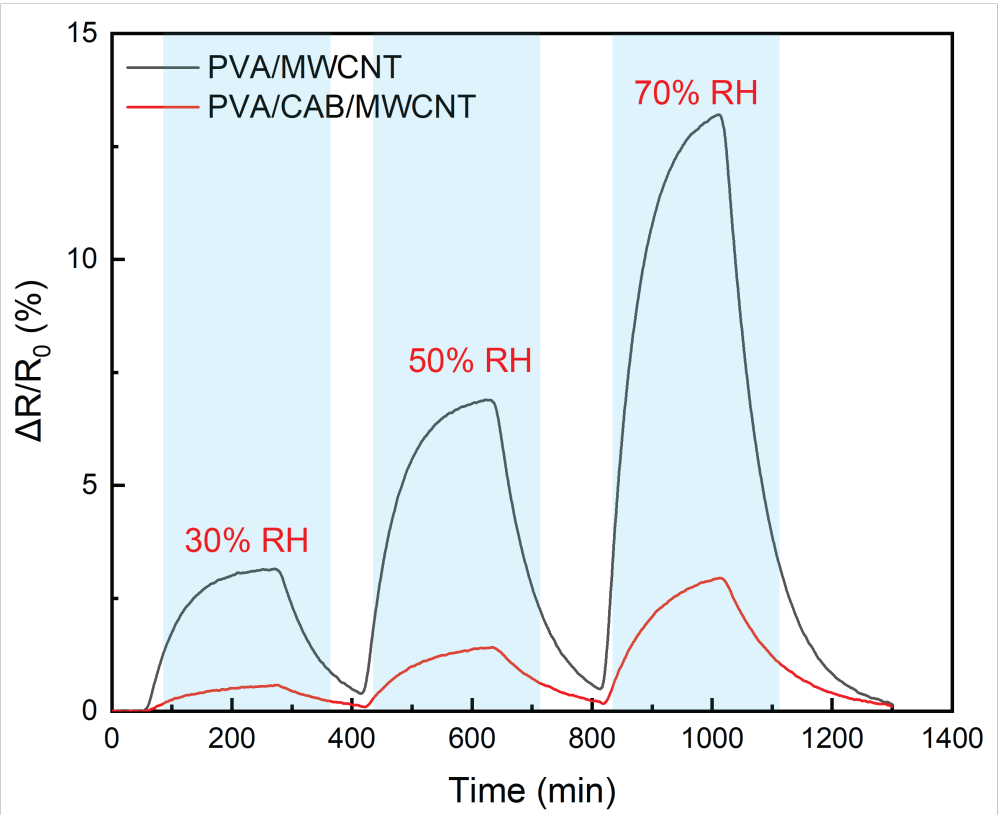

Figure S8: Equilibrium $\Delta R/R_0$ response of PVA/MWCNT (no CAB, black) and PVA3/CAB1/MWCNT03 (red) under stepwise RH exposure at 30%, 50%, and 70% RH. Each RH level was maintained until the resistance reached a stable plateau; dry air recovery was applied between steps. Peak values at 70% RH: PVA/MWCNT ∼13% $\Delta R/R_0$, PVA3/CAB1/MWCNT03 ∼3% $\Delta R/R_0$.

The pure PVA/MWCNT film reaches ∼13% $\Delta R/R_0$ at 70% RH, consistent with its high moisture sensitivity. The PVA3/CAB1/MWCNT03 composite reaches only ∼3% $\Delta R/R_0$ at 70% RH, representing a **70–80% reduction in humidity susceptibility**. This suppression arises from three coupled mechanisms: (i) hydrophobic surface reconstruction by CAB; (ii) partial pre-occupation of PVA hydroxyl sites via PVA–CAB hydrogen bonding; and (iii) diffusion-selective restriction of water uptake in the blended matrix.

References

[1] J. Wang and L. Ye, *Composites Part B: Engineering*, 2015, **69**, 389–396.

[2] M. L. Usrey, A. Chaffee, E. S. Jeng and M. S. Strano, *The Journal of Physical Chemistry C*, 2009, **113**, 9532–9540.

[3] T.-H. Yang and S. J. Lue, *Journal of Macromolecular Science, Part B*, 2013, **52**, 1009–1029.

[4] E. Habeych, X. Guo, J. van Soest, A. J. van der Goot and R. Boom, *Carbohydrate polymers*, 2009, **77**, 703–712.

[5] A. Marzocca, *European polymer journal*, 2007, **43**, 2682–2689.

[6] Y. Eom and B. C. Kim, *Polymer*, 2014, **55**, 2570–2577.

[7] D. M. Kialengila, K. Wolfs, J. Bugalama, A. Van Schepdael and E. Adams, *Journal of Chromatography A*, 2013, **1315**, 167–175.

[8] A. Forster, J. Hempenstall, I. Tucker and T. Rades, *International journal of pharmaceutics*, 2001, **226**, 147–161.

[9] R. Sander, *Atmospheric Chemistry and Physics*, 2023, **23**, 10901–12440.

[10] C. Zhang, A. Jouyban, H. Zhao, A. Farajtabar and W. E. Acree Jr, *Journal of Molecular Liquids*, 2021, **326**, 115219.

[11] S. P. Verevkin, E. L. Krasnykh, T. V. Vasiltsova, B. Koutek, J. Doubsky and A. Heintz, *Fluid Phase Equilibria*, 2003, **206**, 331–339.

[12] W. Mönch, J. Dehnert, E. Jaufmann and H. Zappe, *Applied physics letters*, 2006, **89**, year.

[13] R. E. Pennington and K. A. Kobe, *Journal of the American Chemical Society*, 1957, **79**, 300–305.

[14] M. Yi, Z. Shen, X. Zhang and S. Ma, *Journal of Physics D: Applied Physics*, 2012, **46**, 025301.

[15] R. D. Goodwin, *Journal of Physical and Chemical Reference Data*, 1989, **18**, 1565–1636.

[16] M. Das and D. Sarkar, *Polymer Bulletin*, 2018, **75**, 3109–3125.

[17] X. Duan, Z. Duan, Y. Zhang, B. Liu, X. Li, Q. Zhao, Z. Yuan, Y. Jiang and H. Tai, *Sensors and Actuators B: Chemical*, 2022, **369**, 132302.

[18] V. Inderan, M. M. Arafat, A. S. M. A. Haseeb, K. Sudesh and H. L. Lee, *Nanotechnology*, 2020, **31**, 425503.

[19] P. Molla-Abbasi, *Polymers for Advanced Technologies*, 2022, **33**, 760–769.

[20] V. Anju, P. Jithesh and S. K. Narayanankutty, *Sensors and Actuators A: Physical*, 2019, **285**, 35–44.

[21] Z. Pang, Z. Yang, Y. Chen, J. Zhang, Q. Wang, F. Huang and Q. Wei, *Colloids and Surfaces A: Physicochemical and Engineering Aspects*, 2016, **494**, 248–255.